IL NUOVO CIMENTO Vol. 25 C, N. 2 Marzo-Aprile 2002

Recent results from the Arctic Radiation and Turbulence Interaction STudy (ARTIST) project

M. Nardino, U. Bonafè, F. Calzolari, T. Georgiadis, V. Levizzani
A. Orsini, F. Ravegnani and G. Trivellone

ISAO-CNR, Instituto di Scienze dell'Atmosfera e dell'Oceano
Via Gobetti 101, 40129 Bologna, Italy

(ricevuto il 10 Gennaio 2001; revisionato il 27 Settembre 2001; approvato il 5 Novembre 2001)

Summary. — Ground-based measurements were conducted at Ny-Ålesund in the Svalbard Islands in the framework of the research project ARTIST (Arctic Radiation and Turbulence Interaction STudy) funded by the European Communities. Key objectives of the campaign were: 1) provide all participants with ground reference data as input to models describing the development of the atmospheric boundary level, 2) compute the surface roughness length in order to characterise the surface of the site, 3) parameterise the surface energy exchanges, calculating the surface radiation flux, the sensible and latent heat fluxes, and 4) obtain the surface energy balance during both clear and cloudy sky conditions. The cloud radiative forcing has been also estimated. Final results of the analysis of the data set are presented.

PACS 92.60.Fm – Boundary layer structure and processes.
PACS 92.60.Vb – Solar radiation.
PACS 93.30.Sq – Polar regions.

1. – Introduction

The paramount importance of Polar areas in determining the Earth's climate as well as their environmental susceptibility to climate changes produced on the global scale by anthropogenic activities is one of the most clear-cut results of recent climatic studies. Global Circulation Models (GCMs), in particular, predict substantial warming of the lower atmosphere in the Arctic regions.

Even if these gross results are clearly stated in the literature, GCMs still lack adequate parameterisations of a) the energy exchange between the atmosphere and the surface of the Polar Ocean, and b) the influence of cloud cover, the latter being of fundamental importance in the surface thermodynamics.

The processes governing the variability of sea ice are linked with the energy exchange between low level clouds and the surface. Actually GCMs reflect the inadequacy of current parameterisations showing high differences in terms of mean cloudiness and surface

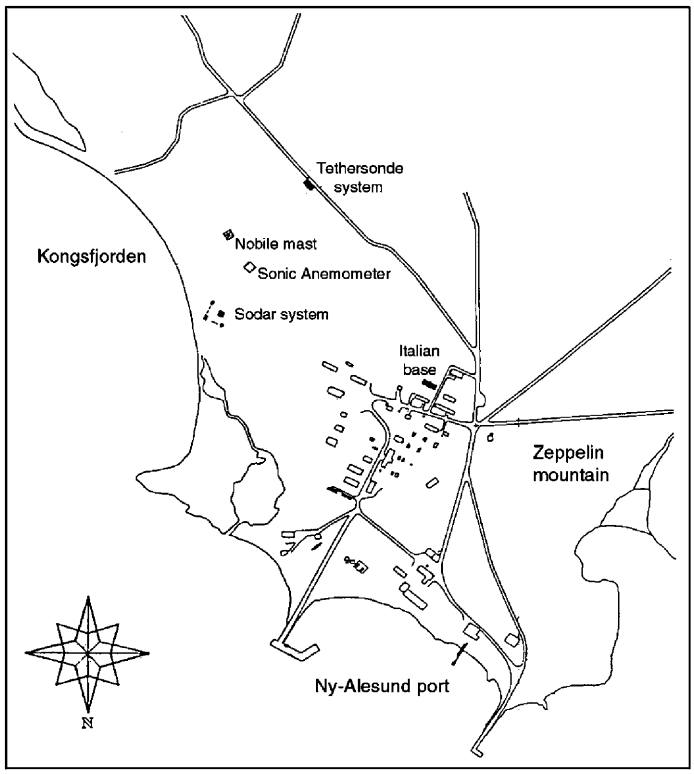

Fig. 1. – Map of the location of the sonic anemometer, radiation station, SODAR and tethersonde systems.

temperature, largely due to the uncertainties in ice-albedo and cloud-radiation feedbacks.

One of the main objectives of the Arctic Radiation and Turbulence Interaction STudy (ARTIST) was the physical parameterisation of surface radiation and energy exchange processes for improving models of the Arctic climate system. An extensive field operation in the Svalbard Islands and the adjacent oceanic regions was conducted in the spring of 1998. During the experiment data were obtained by various aircraft missions, satellite observations, and surface stations.

Results from the analysis of the surface measurements of the ISAO Institute within the frame of the 1998 ARTIST field operation are presented.

2. – Experimental

Measurements were conducted at the Arctic station of Ny-Ålesund (Svalbard Islands, 78°55′N–11°56′E) during the period 19 March-14 April 1998.

A sonic anemometer (Metek, mod. USA-1), a Krypton Hygrometer (Campbell mod. KH2O), and a radiometric station (Kipp and Zonen, mod. CNR-1) equipped with subsurface temperature probes were positioned close to the coastline of the Kongsfijorden (see map in fig. 1).

The radiometric station consists of four different sensors: two pyranometers for measuring the short-wave incoming and outgoing components (CM3 sensors), and two pyrgeometers for the long-wave incoming and outgoing components (CG3 sensors).

Two of the subsurface temperature probes (thermocouples) were buried in the snow at 8 and 17.5 cm depth, respectively, and one at the atmosphere-snow interface.

The radiometric and temperature measurements were recorded by a Campbell CR10ET data-logger every minute, averaged every 10 min and then stored in a Campbell SM192 memory module. Data from the fast sensors (sonic anemometer and hygrometer) were collected at 10 Hz and processed by a Meteoflux computer system (Servizi Territorio).

The experimental equipment was capable of collecting micrometeorological data suitable for the computation of the whole radiation balance as well as the surface energy partition.

3. – Surface roughness length determination

The surface roughness length z_0 is a key parameter characterising the dynamic forcing of the surface on the atmospheric flow. It is defined as the height at which the logarithmic wind profile approaches the zero speed value [1]. Ice surfaces have a highly variable value of z_0 depending on surface texture.

The surface roughness length may be derived from the vertical wind speed profile, which is described by the similarity theory as follows:

$$u_z = \frac{u_*}{k}\left[\ln\left(\frac{z}{z_0}\right) - \Psi_m\left(\frac{z}{L}\right)\right], \tag{1}$$

where the similarity universal function Ψ_m changes its form as a function of the atmospheric stability:

– in convective conditions ($z/L < 0$)

$$\Psi_m\left(\frac{z}{L}\right) = \ln\left[\left(\frac{1+x^2}{2}\right)\left(\frac{1+x}{2}\right)^2\right] - 2\arctan(x) + \frac{\pi}{2}, \tag{2a}$$

where

$$x = \left(1 - a_1\frac{z}{L}\right)^{1/4}; \tag{2b}$$

– in adiabatic conditions ($z/L = 0$)

$$\Psi_m\left(\frac{z}{L}\right) = 0; \tag{3}$$

– in stable conditions ($z/L > 0$)

$$\Psi_m\left(\frac{z}{L}\right) = -a_2\left[1 - \exp\left[-a_3\frac{z}{L}\right]\right]. \tag{4}$$

The constants a_1, a_2 and a_3 were taken equal to 16, 17 and 0.29, respectively [2]. For the calculation of z_0 it is necessary to know the horizontal wind speed u, the friction

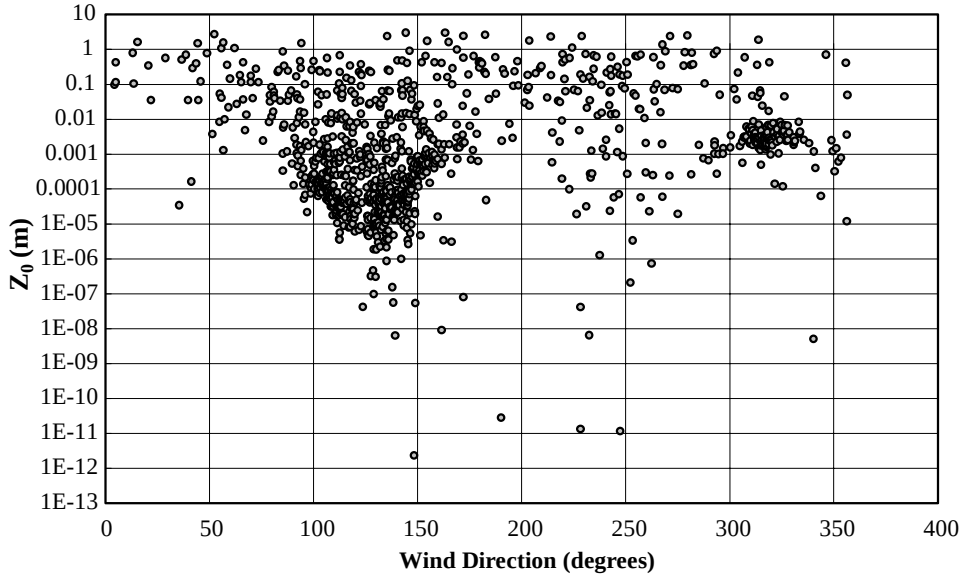

Fig. 2. – Values of the surface roughness length as a function of the wind direction.

velocity u_* and the stability parameter z/L for the whole period. These quantities were derived from sonic anemometer measurements, which were available throughout the campaign.

The data set was subdivided with respect to the wind direction by slicing 36 wind sectors. For each i-th sector the corresponding N_j measurements were considered:

$$\left\langle u_k^j, (u_*)_k^j, L_k^j \right\rangle, \qquad k = 1, 2, ..., N_j \, .$$

From eq. (1) and for each of the variables N_j we have computed:

$$y_k^j = [\ln(z_0)]_k^j = \ln(z) - \frac{k u_k^j}{(u_*)_k^j} - \Psi_m \left(\frac{z}{L}\right) . \tag{5}$$

Finally, the value of z_0 was expressed by

$$z_0 = \exp\left[y_k^j\right] , \tag{6}$$

where z_0 was computed for all 36 sectors by a FORTRAN program used for the processing of the data [3].

The values of the surface roughness length are shown in fig. 2 as a function of the wind direction. As from previous studies in Antarctica [4] the scatter of z_0 is extremely high (12 orders of magnitude) indicating strong variations in the surface conditions and effects due to snow drift.

A value of z_0 for each wind sector was computed to characterise the surface around the measurement site. Two methods for the determination of the appropriate z_0 are

TABLE I. – *Mean and median values of surface roughness length for each wind sector.*

Wind sector (°)	Number of data	Mean value of z_0 (m)	Median value of z_0 (m)
5	4	$2.1 \cdot 10^{-1}$	$1.1 \cdot 10^{-1}$
15	4	$8.4 \cdot 10^{-1}$	$1.0 \cdot 10^{-1}$
25	5	$3.1 \cdot 10^{-1}$	$3.4 \cdot 10^{-1}$
35	5	$2.4 \cdot 10^{-1}$	$3.4 \cdot 10^{-2}$
45	7	$4.4 \cdot 10^{-1}$	$2.9 \cdot 10^{-1}$
55	12	$4.9 \cdot 10^{-1}$	$4.6 \cdot 10^{-2}$
65	14	$2.1 \cdot 10^{-1}$	$1.1 \cdot 10^{-2}$
75	8	$7.5 \cdot 10^{-2}$	$3.9 \cdot 10^{-2}$
85	26	$1.1 \cdot 10^{-1}$	$4.0 \cdot 10^{-2}$
95	48	$6.7 \cdot 10^{-2}$	$1.2 \cdot 10^{-3}$
105	112	$1.8 \cdot 10^{-1}$	$1.8 \cdot 10^{-4}$
115	109	$2.1 \cdot 10^{-2}$	$1.0 \cdot 10^{-4}$
125	94	$1.8 \cdot 10^{-2}$	$7.0 \cdot 10^{-5}$
135	138	$2.4 \cdot 10^{-2}$	$4.0 \cdot 10^{-5}$
145	118	$5.4 \cdot 10^{-2}$	$1.3 \cdot 10^{-4}$
155	66	$5.7 \cdot 10^{-2}$	$7.0 \cdot 10^{-4}$
165	29	$2.8 \cdot 10^{-1}$	$1.9 \cdot 10^{-3}$
175	23	$2.3 \cdot 10^{-1}$	$5.0 \cdot 10^{-2}$
185	12	$4.9 \cdot 10^{-1}$	$3.0 \cdot 10^{-1}$
195	13	$1.3 \cdot 10^{-1}$	$9.1 \cdot 10^{-2}$
205	10	$3.3 \cdot 10^{-1}$	$1.8 \cdot 10^{-1}$
215	13	$3.1 \cdot 10^{-1}$	$3.2 \cdot 10^{-2}$
225	14	$3.5 \cdot 10^{-1}$	$6.8 \cdot 10^{-2}$
235	23	$1.4 \cdot 10^{-1}$	$1.5 \cdot 10^{-2}$
245	34	$9.6 \cdot 10^{-2}$	$1.9 \cdot 10^{-2}$
255	29	$1.6 \cdot 10^{-1}$	$1.9 \cdot 10^{-2}$
265	18	$2.4 \cdot 10^{-1}$	$5.0 \cdot 10^{-2}$
275	9	$7.7 \cdot 10^{-1}$	$2.0 \cdot 10^{-1}$
285	9	$2.0 \cdot 10^{-1}$	$5.2 \cdot 10^{-2}$
295	10	$1.6 \cdot 10^{-1}$	$1.6 \cdot 10^{-3}$
305	20	$5.2 \cdot 10^{-2}$	$3.1 \cdot 10^{-3}$
315	63	$4.8 \cdot 10^{-2}$	$3.0 \cdot 10^{-3}$
325	32	$5.0 \cdot 10^{-3}$	$3.6 \cdot 10^{-3}$
335	10	$3.3 \cdot 10^{-3}$	$2.6 \cdot 10^{-3}$
345	9	$9.9 \cdot 10^{-2}$	$1.1 \cdot 10^{-3}$
355	12	$5.7 \cdot 10^{-2}$	$1.2 \cdot 10^{-4}$

proposed in the literature: 1) the mean value, and 2) the median value. We calculated these two values for each wind sector and the results are presented in table I and in fig. 3.

Note from table I that the median values are distinctly smaller than the corresponding mean values, and they are closer to the values for rather smooth snow and ice surfaces. The median values vary between a minimum of 4×10^{-5} m and a maximum of 0.34 m. The maximum value is by far too high for a snow surface, but this can be due to the location of the instruments. In fact, the SODAR system (IFA-CNR, Rome) was located close to the sonic anemometer and this certainly perturbed the surface roughness measurements. The highest values of z_0 show up when the number of data of a certain wind sector is

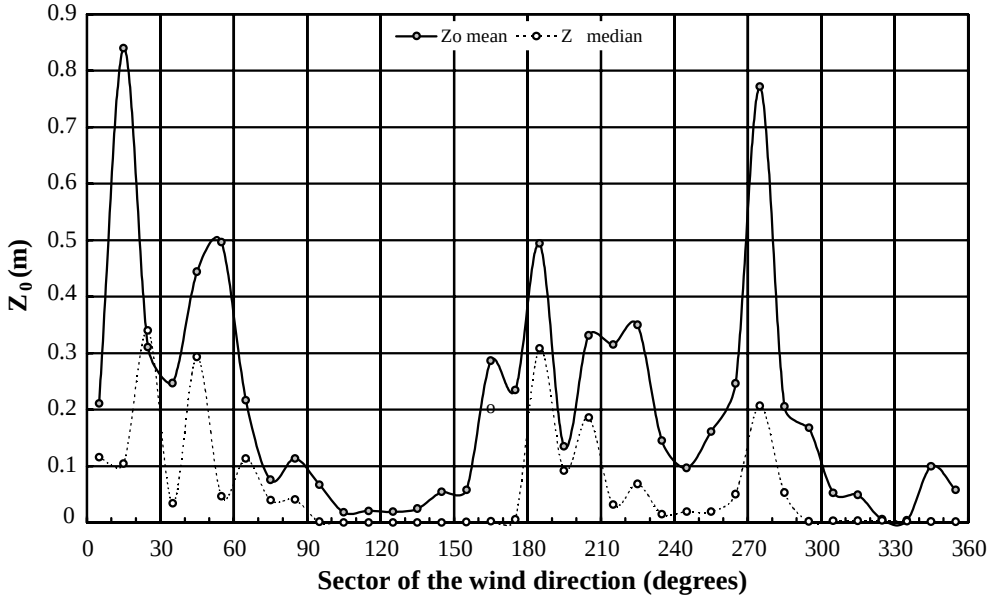

Fig. 3. – Mean and median values of the surface roughness length as a function of the wind direction sector.

limited (less than 20). Another reason for the high values is that the results are unreliable when the wind speed is very low (< 3 m s^{-1}).

Therefore, we suggest the low values in the sectors 90° to 180° and 300° to 360° represent the best surface characteristics for the study.

4. – The turbulent fluxes

The surface turbulent fluxes have been calculated from the sonic anemometer measurements through the eddy-correlation technique.

The time series of the turbulent kinetic energy (TKE), representing the turbulence intensity, is shown in fig. 4a. The highest values occur during high wind speed events in correspondence with the highest fluxes of momentum (fig. 4b) and sensible heat (fig. 4c).

The momentum and sensible heat fluxes are terms of the TKE budget equation, so that an increase of turbulence results in an increase of surface stress as well as of the sensible heat.

The sensible heat flux is primarily downward. Only during the last period of the campaign, which is characterised by a limited cloud coverage, the sensible heat flux (fig. 4c) tends to assume positive values (convective atmospheric conditions).

Since the equipment for the derivation of the turbulent latent heat flux did not work properly, LE was calculated from the bulk formula

$$LE = \rho\lambda C_E \left(q_\mathrm{S} - q_\mathrm{a}\right) V \,, \tag{7}$$

where λ is the sum of enthalpies of melting and vaporisation, C_E the vapour transfer coefficient, q_s the saturation specific humidity at the surface, q_a the specific humidity of

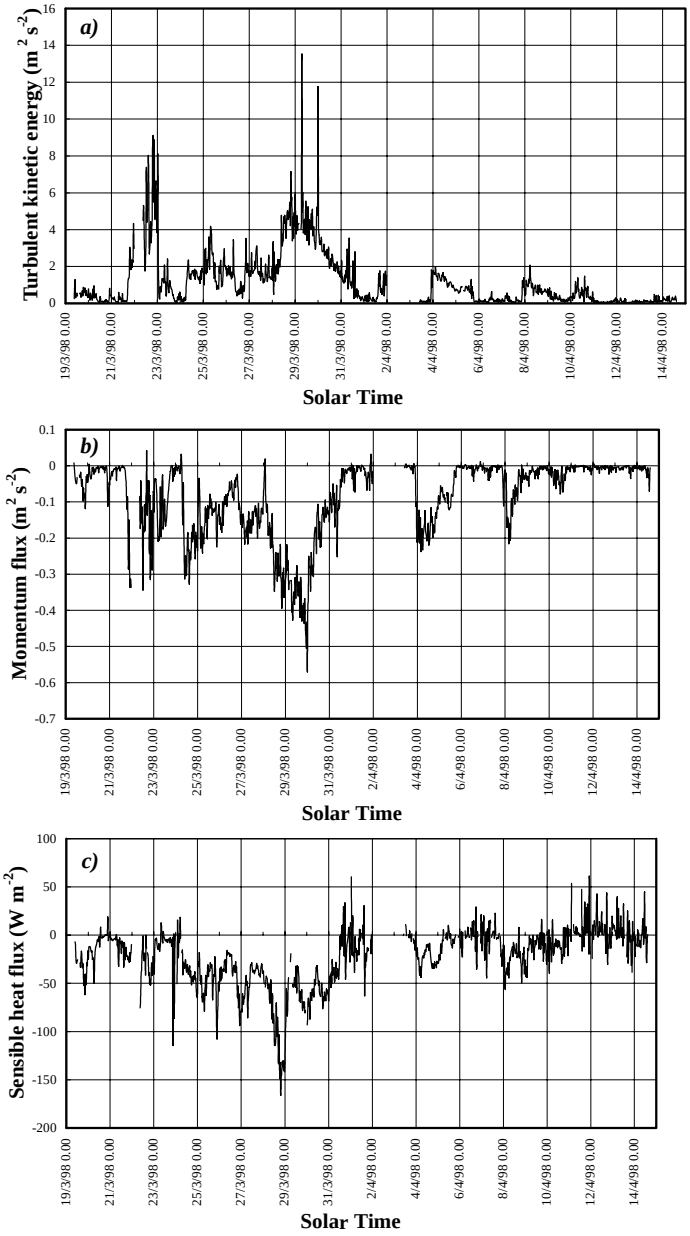

Fig. 4. – Time series of: a) the turbulent kinetic energy; b) the momentum flux; c) the sensible heat flux.

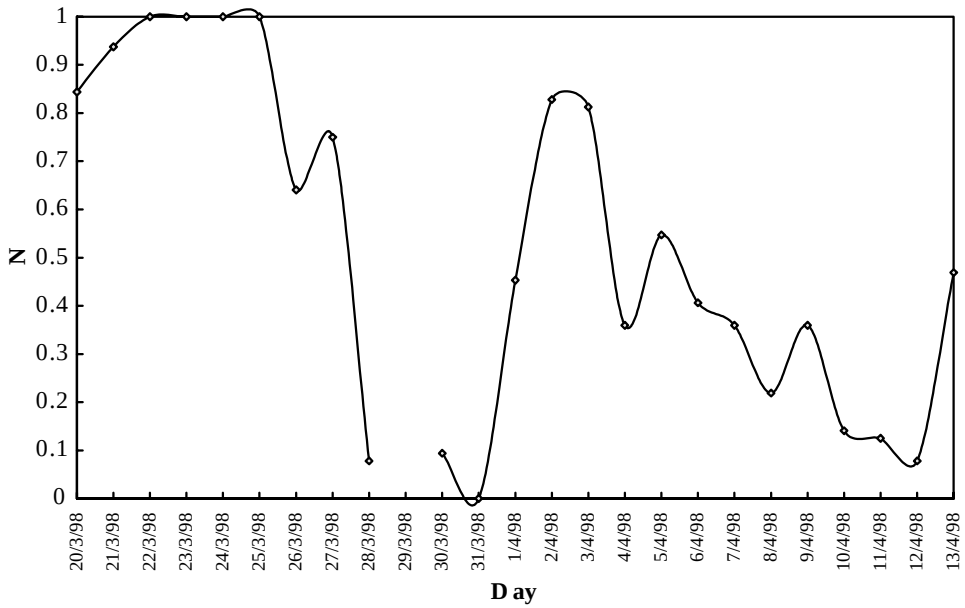

Fig. 5. – Daily mean cloud fraction.

the air at 2 m height, and V the wind speed at the same level. q_{a} was calculated from the Koldewey synoptic station data of air temperature and relative humidity. Since the transfer coefficient C_E in eq. (7) depends on LE, the equation was solved iteratively [5].

5. – Influence of cloud cover on the surface radiation budget

The cloud fraction (N) decreases during the campaign (see fig. 5) and this strongly affects the longwave radiation balance (Lwn) (fig. 6).

Note that Lwn increases with increasing cloudiness from about -70 W m^{-2} to -10 W m^{-2}. The best linear fit provides the best estimate of the relationship.

In order to investigate the dependence of the net shortwave radiation on N, it needs to separate the effect of clouds by the progressive enhancement of incoming shortwave radiation associated to the increase of the solar elevation during the campaign. For this purpose, the shortwave net radiation has been normalised subtracting a reference value from each observed value. The reference value represents the amount of shortwave net radiation that would be expected at the surface in cloudless conditions:

$$Swn(\text{normalised}) = Swn(\text{observed}) - Swn(\text{reference})\,. \tag{8}$$

The reference value has been calculated using the following expression:

$$Swn(\text{reference}) = Sw_{\mathrm{TOA}}(1-\overline{\alpha_{\mathrm{cl}}}) \cdot \overline{\left[\frac{Swn(\text{observed})}{Sw_{\mathrm{TOA}}(1-\overline{\alpha})}\right]_{\mathrm{cl}}}\,, \tag{9}$$

where Sw_{TOA} is the incoming shortwave radiation at the top of the atmosphere (TOA) and $\overline{\alpha_{\mathrm{cl}}}$ is the mean clear-sky albedo. The last term is the mean of the ratio in square

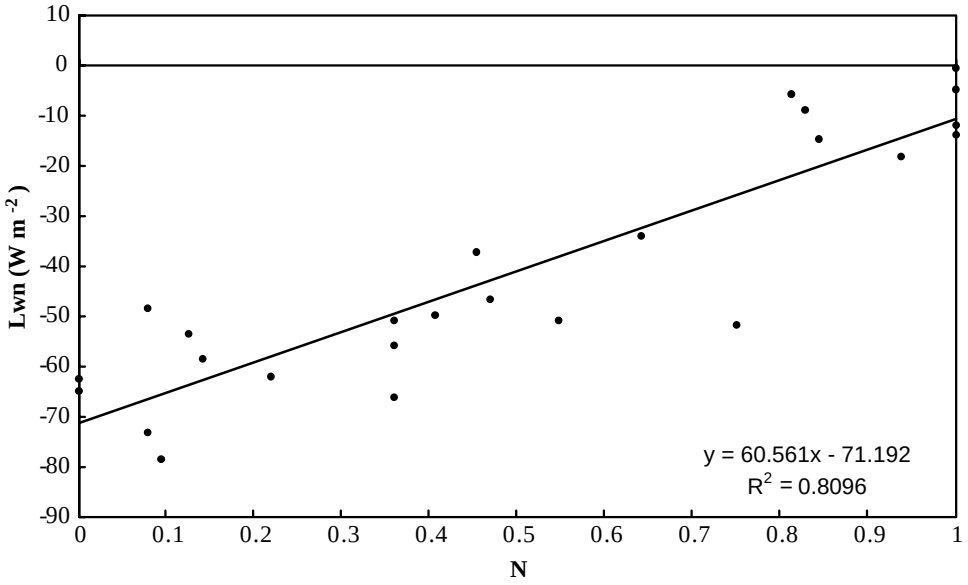

Fig. 6. – Dependence of the daily mean net longwave radiation (Lwn) on cloud fraction.

parenthesis calculated for cloudless days.

In fig. 7 the daily mean values of the normalised net shortwave radiation are plotted against the cloud fraction values. The decrease of Swn (normalised) with N, obtained

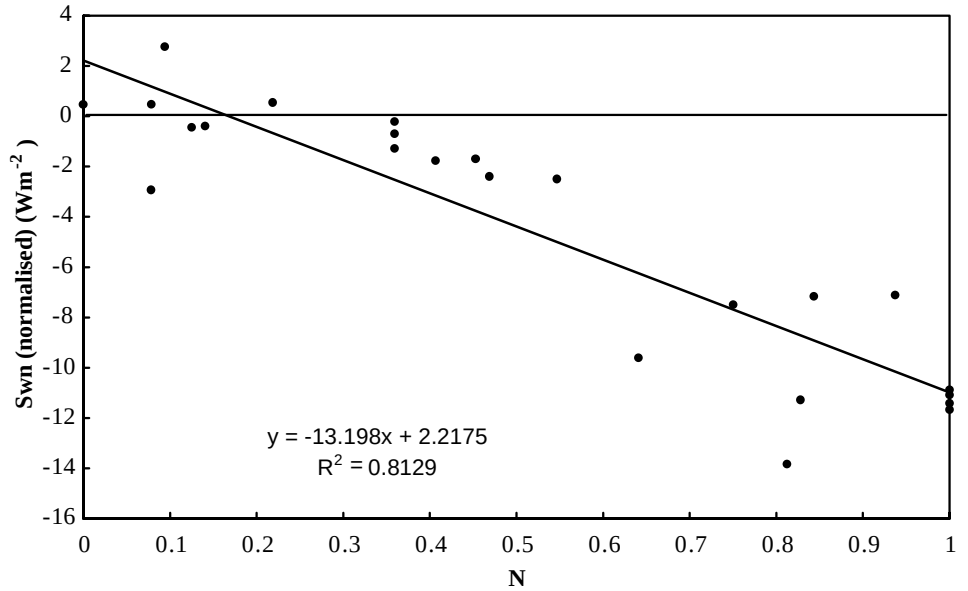

Fig. 7. – Dependence of the normalised daily mean net shortwave radiation obtained with eq. (8) on the cloud fraction N.

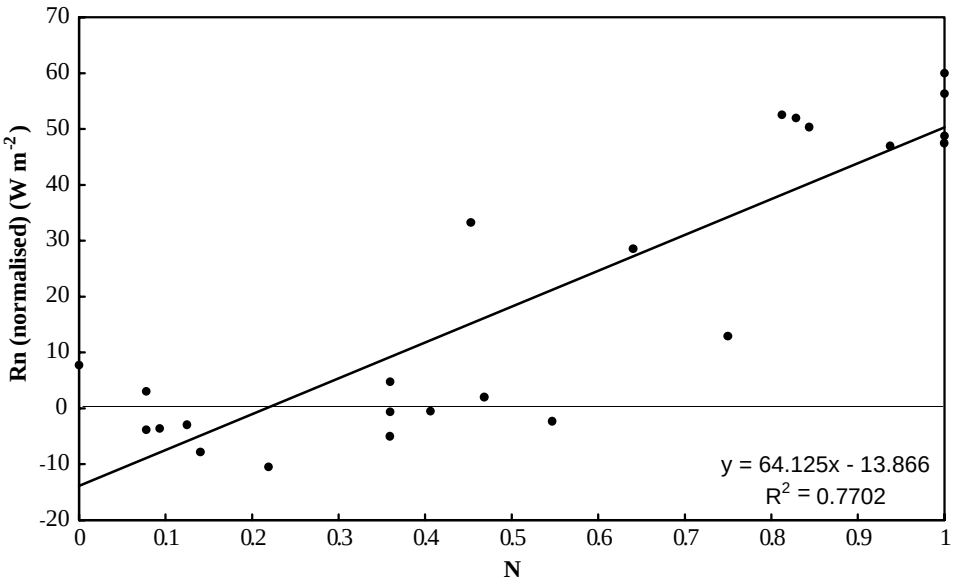

Fig. 8. – Dependence of the normalised daily mean net radiation obtained with eq. (10) on the cloud fraction N.

calculating the linear best fit of the data, is about -13 W m^{-2} from clear to overcast skies.

The net radiation Rn needs also to be normalised as follows:

$$Rn(\text{normalised}) = Rn(\text{observed}) - (\overline{Lwn_{\text{cl}}} + Swn(\text{reference}))\,, \tag{10}$$

where $\overline{Lwn_{\text{cl}}}$ is the mean longwave net radiation on clear days.

Figure 8 shows that the daily mean net radiation normalised with eq. (10) increases with increasing cloud fraction.

In general during the entire campaign the dependence of the net radiation on cloud amount is mainly influenced by the variation of the longwave radiation with N. During this period of the year at Ny-Ålesund longwave radiation is the predominating term in the net radiation balance, particularly in clear-sky conditions.

The analysis of the linear relationship between the daily mean values of the net longwave, shortwave and total radiation and the cloud fraction provides only a first estimate of their interdependence during the period of measurement. More details on the effects of clouds on the surface radiation budget are necessarily obtained by considering the variation of the instantaneous values. The dependence of the normalised Rn taken every three hours on cloud fraction is shown in fig. 9.

For $N \leqslant 0.5$, 68% of the normalised Rn values are negative, *i.e.* the observed values are smaller than the corresponding reference values expected in clear-sky condition.

In contrast, for $N > 0.5$, 81% of the normalised Rn values are positive, *i.e.* the observed values are larger than the corresponding reference values. This seems to indicate that for $N \leqslant 0.5$ the presence of clouds lead to a decrease in the surface net radiation, and for $N > 0.5$ the overall effect results as an increase in the surface energy availability.

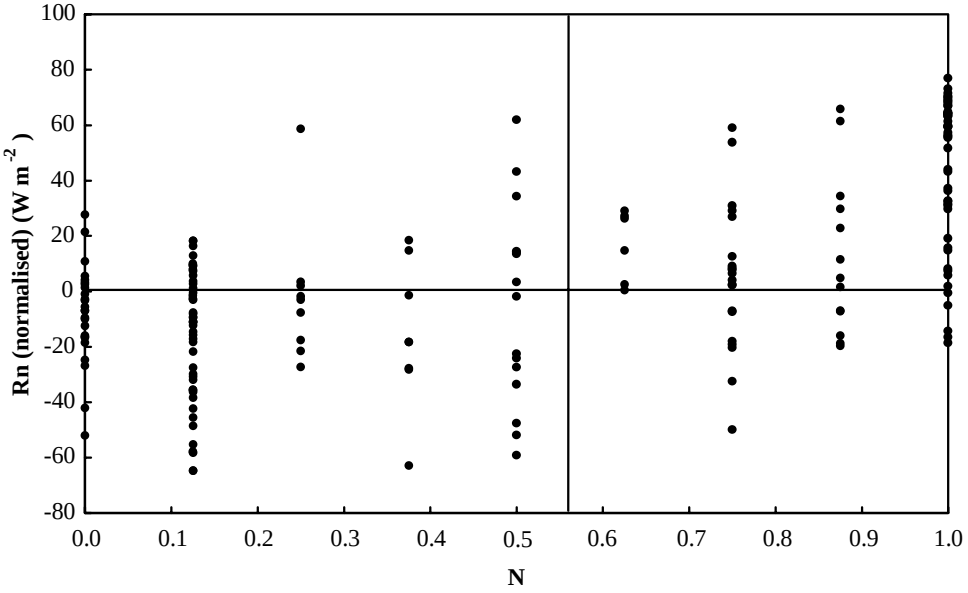

Fig. 9. – Dependence of the normalised Rn on the cloud fraction N for data collected every three hours.

Data collected during the campaign are too few to reach a firm conclusion. For small values of N, the increase of the net longwave radiation with N is smaller than the decrease of the net shortwave radiation. It is thus reasonable to assume that these two effects do not occur at a fixed N, but seem to be ascribable to the ratio between the absolute values of the net shortwave and longwave radiation.

An analysis of more data at the beginning of the spring season becomes necessary for a better understanding of the dependence of Rn on N in these rather peculiar conditions, *i.e.* when the absolute value of net shortwave radiation is smaller than the absolute value of net longwave radiation.

6. – The surface energy balance on a clear and a cloudy day

In general, it was found that the energy balance is closer to zero when all energy fluxes are low, when the air temperature is less than $-10°$C and the wind is blowing from NW at a speed lower than 5–6 m s^{-1}. Figure 10 shows values for a clear-sky and an overcast day (8 April and 20 March, respectively) that obey to these characteristics. The overcast day is characterised by a warm and cloudy atmosphere during which the turbulent and conductive fluxes are well balanced by the net radiation.

In clear-sky conditions the net radiation has a distinct diurnal cycle which extends to the net energy balance, the latter being nearly negative all the time.

In fig. 11 the scatter plots of the differences between the net radiation and the sub-surface energy flux are plotted against the turbulent fluxes with the inverted signs for 8 April and 20 March. The straight lines indicate the best linear fit to the data, and R is the correlation coefficient. On the clear day the values are much more scattered than on the overcast day as expressed by R. In both cases, however, the equations of the linear

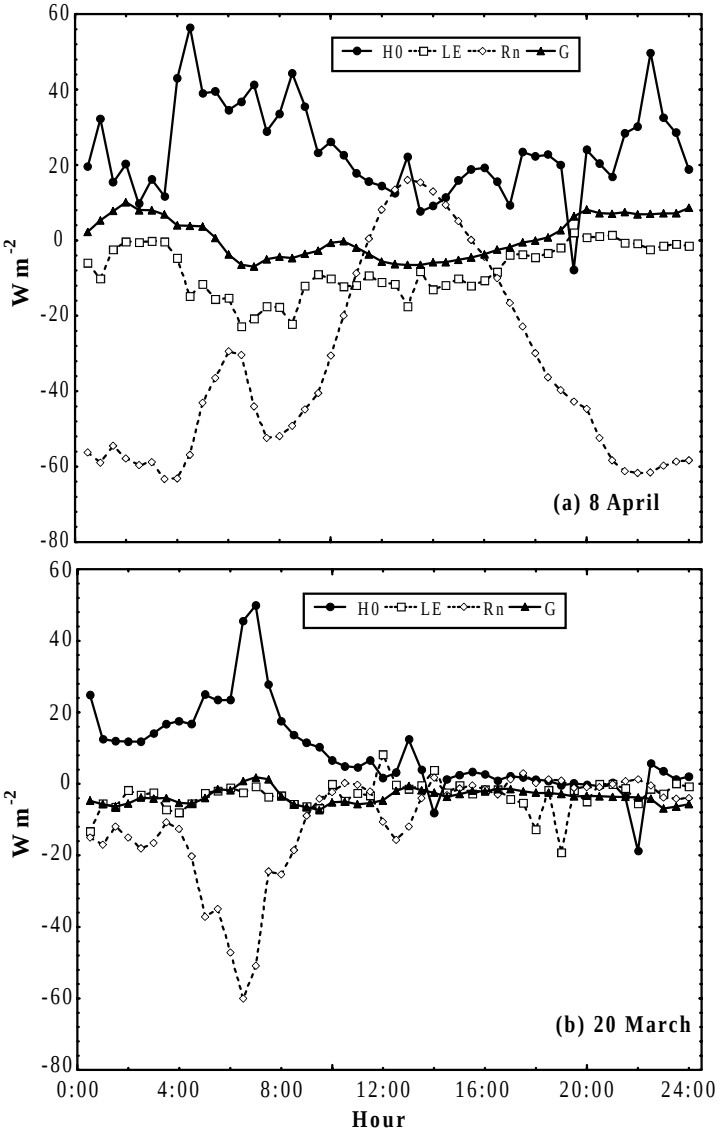

Fig. 10. – Energy balance terms calculated on a clear-sky (8 April) and an overcast-sky day (20 March).

best fit indicate that the difference between $(Rn - G)$ and $(-H - LE)$ is smaller than the experimental errors.

7. – Conclusions

The observation site of Ny Ålesund is characterised by a complex topography due to the fjord and mountains. This had obvious effects on the distribution of wind direction and speed, which were influenced by the large-scale pressure field, topographical chan-

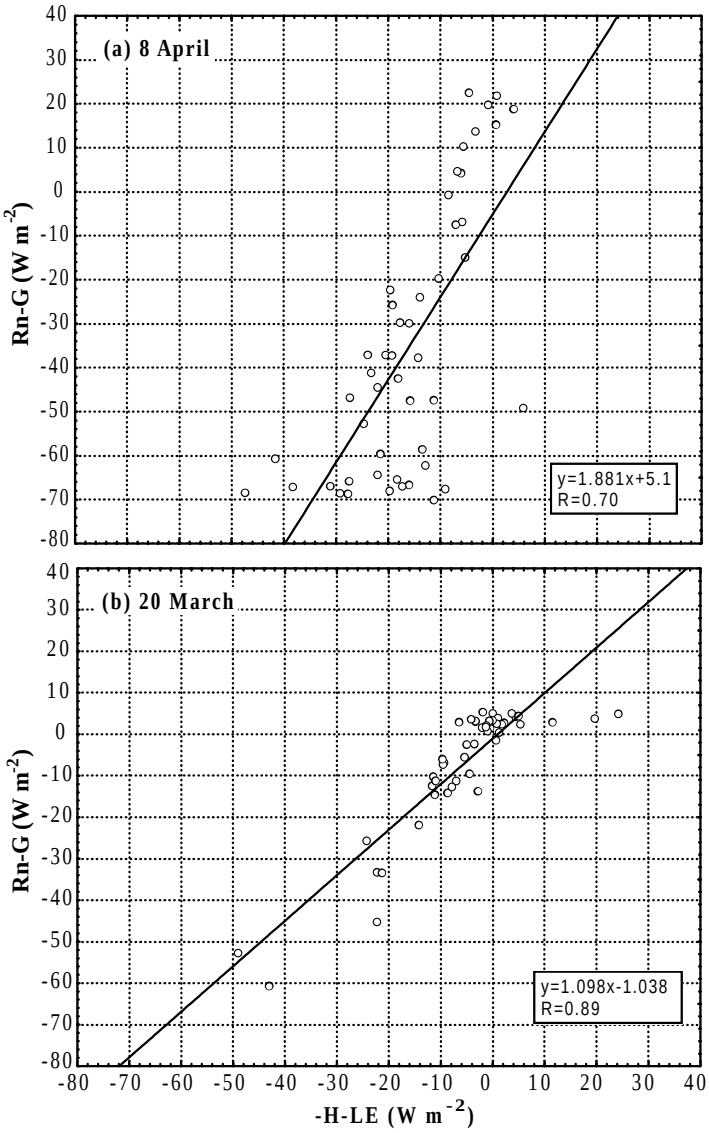

Fig. 11. – 1:1 plot of the difference between Rn and G against the turbulence fluxes H and LE with the inverted signs, for 8 April (a) and 20 March (b).

nelling, and the occurrence of katabatic winds. The observation period was characterised by varying weather conditions: a 17-day period of cloudy skies with strong winds was followed by 10 days of clear skies with low winds. These large-scale events were strongly reflected by the surface energy balance, with large downward turbulent momentum and sensible heat fluxes during the first period, and corresponding small fluxes during the second period.

The turbulence measurements yielded an overall aerodynamic roughness length of

1.3×10^{-4} m corresponding to a neutral 10 m drag coefficient of 1.3×10^{-3}, which is well comparable with previous observations over snow and ice surfaces. The atmospheric surface layer stability varied from $-2 < 10/L < 2$, and most of the cases outside the near-neutral region occurred in correspondence of wind velocities smaller than 4 m s^{-1}. During the cloudy and windy period, the sensible heat flux reached a peak value of 150 W m^{-2} directed downward.

The surface radiation balance was dominated by the net longwave radiative flux, and the mean value of the surface net radiation was consequently negative. A first analysis of the cloud effect on the radiation balance seems to show that the total net radiation decreased with cloud fraction (N) for small cloud amounts ($N < 0.5$), but increased with N when more clouds were present. The surface albedo showed a cloud dependence, increasing with an increasing cloud fraction.

The heat flux in the snow was calculated from the time series of the temperature profile down to 0.2 m. The results demonstrated the importance of the heat conduction and absorption of solar radiation below the snow surface.

In general, our opinion is that the present measurements form an important data set for an accurate characterisation of the Ny-Ålesund Arctic site in terms of radiative and turbulent exchange processes. The results have a potential importance for development of parameterisation schemes for climate and weather forecasting models.

We have no doubt of the relevant character of the data set for Arctic studies, because not many comparable sets of measurements are available in the literature or in data banks due to the difficulties in setting up experimental stations in these remote areas whose climatic and meteorological conditions are often very harsh. This is why a permanent scientific base needs to be established if one wants to perform long series of measurements, during which the instrumentation has to be carefully tested and periodically checked.

* * *

The study was funded by European Commission DGXII within the 4th Framework Programme "Environment and Climate" (Contract n. ENV4-CT97-0487). The authors wish to thank "CNR- Progetto Strategico Artide" and in particular Mr. R. Sparapani (CNR-IIA) for his factual support to the study solving all the logistic problems that occurred at the site.

REFERENCES

[1] Andreas E. L., *Boundary-Layer Meteorol.*, **38** (1987) 159.
[2] Sozzi R., Favaron M. and Georgiadis T., *J. Appl. Meteorol.*, **37** (1998) 461.
[3] Nardino M., Pirazzini R., Georgiadis T., Levizzani V., Vihma T., Cheng B., Calzolari F., Ravegnani F., Trivellone G. and Bonafè U., *Ground based radiation and turbulence measurements at Ny Alesund (Svalbard): First data analysis and modelling*, CNR-Polar Atmospheres Report No PAS-1/2000 (Roma) 2000, p. 92.
[4] Bintanja R. and Van den Broeke M. R., *Boundary-Layer Meteorol.*, **74** (1995) 89.
[5] Launiainen J. and Vihma T., *Environmental Software*, **5** (1990) 113.